The Journal of Chemical Physics

RESEARCH ARTICLE | SEPTEMBER 03 2024

Two stage decoherence of optical phonons in long oligomers

Alexander L. Burin ; Igor V. Rubtsov

J. Chem. Phys. 161, 094901 (2024)
https://doi.org/10.1063/5.0222580

The Journal of Chemical Physics ARTICLE pubs.aip.org/aip/jcp

Two stage decoherence of optical phonons in long oligomers

Cite as: J. Chem. Phys. 161, 094901 (2024); doi: 10.1063/5.0222580
Submitted: 8 June 2024 • Accepted: 13 August 2024 •
Published Online: 3 September 2024

Alexander L. Burin[a] and Igor V. Rubtsov

AFFILIATIONS

Department of Chemistry, Tulane University, New Orleans, Louisiana 70118, USA

[a]Author to whom correspondence should be addressed: aburin@tulane.edu

ABSTRACT

Molecular vibrations are generally responsible for chemical energy transport and dissipation in molecular systems. This transport is fast and efficient if energy is transferred by optical phonons in periodic oligomers, but its efficiency is limited by decoherence emerging due to anharmonic interactions with acoustic phonons. Using a general theoretical model, we show that in the most common case of the optical phonon band being narrower than the acoustic bands, decoherence takes place in two stages. The faster stage involves optical phonon multiple forward scattering due to absorption and emission of transverse acoustic phonons, i.e., collective bending modes with a quadratic spectrum; the transport remains ballistic and the speed can be altered. The subsequent slower stage involves phonon backscattering in multiphonon processes involving two or more acoustic phonons resulting in a switch to diffusive transport. If the initially excited optical phonon possesses a relatively small group velocity, then it is accelerated in the first stage due to its transitions to states propagating faster. This theoretical expectation is consistent with the recent measurements of optical phonon transport velocity in alkane chains, increasing with increasing the chain length.

I. INTRODUCTION

Molecular vibrations are significant for chemical energy transport and dissipation;[1–5] they control reaction kinetics[6,7] and have potential applications in several fields of modern technology spanning from sustainable energy to biomedicine to thermal management.[2,8–12] Energy transport can be fast and efficient even compared to that in metals because it emerges due to covalent bonds, which are the strongest chemical bonds existing in nature.[2,9–12] Although thermal conductivity of molecules at room temperature or below is determined substantially by low energy acoustic phonons,[9,12–14] high energy optical phonons can facilitate chemical energy transport.[4,15,16] Indeed, typical chemical energy, exceeding phonon energy by over an order of magnitude, can be released easier to optical phonons rather than to acoustic phonons possessing considerably smaller energy. Since their propagation speeds are comparable,[17] optical phonons can transfer energy more efficiently compared to the acoustic ones.

The fast and efficient energy transport by optical phonons has been demonstrated in numerous experiments.[15,18–22] If an optical phonon is initiated within the band of a periodic oligomer chain, it can propagate along the chain ballistically due to normal mode delocalization.[15] This is the most efficient energy transport realization, which is limited by decoherence and relaxation of propagating phonons induced by their anharmonic interactions with the other intramolecular vibrations and the environment.[17] Here, we consider intramolecular interactions since the coupling to the environment is much weaker.[5]

Following earlier work,[23] we specify that optical transitions within the phonon band lead to decoherence, while those out of the phonon band lead to irreversible relaxation. Decoherence occurs inevitably due to interaction with low frequency acoustic phonons, while relaxation requires involvement of other optical phonons and is usually slower.[23–25] Consequently, decoherence is the first possible source of ballistic transport breakdown to consider. In the present work, *we focus on optical phonon decoherence due to their anharmonic interaction with transverse acoustic phonons.*

Decoherence induced by interaction with longitudinal or torsional acoustic phonons possessing a linear spectrum $\omega \approx ck$ (where ω is a phonon frequency, k is its wavevector, and c is the speed of sound) was considered in earlier work.[17] It was shown there that the optical phonon decoherence is substantially suppressed in the most common situation of a forbidden Cherenkov's like emission (or absorption), where the speed of sound c exceeds the maximum optical phonon velocity $v_{\max}$. In this regime, only relatively slow high order anharmonic processes (fourth and higher) result in phonon

scattering in contrast with the regime of a violated Cherenkov's constraint $v_{max} > c$.

Decoherence due to transverse acoustic phonons representing collective bending modes needs special consideration because these phonons possess a quadratic spectrum at small wavevectors ($\omega = Aq^2$, see, e.g., Ref. 26). For this spectrum, there always exist acoustic phonons with a small velocity violating Cherenkov's constraint, so absorption and emission are always allowed. However, if an optical phonon band is narrower than that for transverse acoustic phonons, then the absorption or emission of transverse phonons leads to a small change in the optical phonon wavevector compared to this wavevector. Consequently, absorption or emission does not modify the direction of the optical phonon propagation, leading only to its forward scattering. Backscattering requires multiphonon processes occurring much slower compared to single phonon absorption or emission. Thus, phonon relaxation occurs in two (fast and slow) stages. The fast stage taking around 1–10 ps involves an incomplete equilibration of the optical phonon within the states of the band with group velocities oriented toward its initial direction. At that stage, the energy propagates with a nearly constant velocity similarly to the ballistic transport regime. The second stage, involving phonon backscattering, emerges after orders of magnitude longer time. Only at that stage, the transport mechanism changes from the ballistic transport to the diffusive transport. Acoustic bands are usually wider than optical bands since they are determined by direct atomic interactions through covalent bonds (see, e.g., Refs. 17 and 24), so two stages of decoherence should take place for most of the optical phonon bands.

If the acoustic band is narrower than the optical phonon band, then the optical phonon relaxes very quickly in about few picoseconds from its initial state to all other states within the band. This relaxation leads to substantial current reduction and changing the transport from ballistic to diffusive. This regime is not expected for optical phonons, but it is relevant for other systems of interest, including electrons propagating in periodic molecules.

Optical phonon velocities that are initially slower than normal have been observed to accelerate during the first stage. This increase can be used to interpret the observations of Ref. 27 in alkane chains, where an increase in the optical phonon transport velocity has been discovered with increasing the chain length. In the opposite case of a narrow transverse phonon band, any absorption or emission of transverse phonons overturns the propagating phonon backward, leading to a rapid ballistic transport breakdown similarly to Ref. 17.

To summarize the main goal of the present work is to characterize the optical phonon transport affected by the interaction with transverse acoustic phonons. To characterize the transport, we present a theoretical model describing the interactions between the optical phonon and transverse acoustic phonons. We will model both sets of modes as collections of harmonic oscillators $|o\rangle|a\rangle$. Here, $|o\rangle$ represents an optical phonon state (normal mode) and $|a\rangle$ likewise represents a direct product of transverse acoustic phonon states. The frequencies of both sets are chosen to form optical and acoustic energy bands. Cubic anharmonic couplings, bilinear in the optical mode and linear in the acoustic mode, are introduced to allow near resonant energy in which an $|o\rangle|a\rangle$ state is coupled to another nearly degenerate $|o'\rangle|a'\rangle$ state. The dynamics of the model is studied at three different levels of theory with the goal of highlighting how coupling strengths, densities of states, temperature, and the widths of the two bands influence energy transport.

Our consideration is limited to a single excited optical phonon. This is the regime realized in the 2D IR experiments,[15,23–25] where the optical phonons are excited by the infrared laser pulse. The heat released during, for example, chemical reaction would be transported by more than single optical phonon. Yet the scattering of optical phonon by acoustic phonons can be characterized using the consideration of the present work.

This paper is organized as follows: In Sec. II, the model of optical and transverse acoustic phonons and their anharmonic interactions is introduced. In Sec. III, the phonon decoherence is considered in terms of elementary processes of transverse phonon emission, absorption or scattering. The rates of these processes are estimated using the Fermi golden rule, and the regimes of the Fermi golden rule failure are discussed. Our estimates are found to be consistent with the numerical simulations reported in Sec. IV and targeted to verify the predictions of Sec. III. These simulations are performed using accurate quantum mechanical[17,28] and semiclassical[29] approaches for low and high temperature limits. In Sec. V, we numerically examine the increase in the transport speed of optical phonon with the time assuming its small initial velocity and discuss the possible connection of this result to recent experiments in alkane chains.[27] Finally, the conclusions are formulated in Sec. VI.

We ignore any static disorder, for instance gauche kinks in alkane chains. The kinks can remarkably affect the phonon transport because they reflect propagating phonons backward.[30] We ignore them assuming that the temperature is sufficiently small, so most of the molecules do not have these kinks at room temperature. This is consistent with the estimate in Ref. 30 for the molecular length below 15 nm.

II. MODEL

Here, we introduce the model for optical phonons in a periodic chain interacting with transverse acoustic phonons. Our consideration is limited to a single optical phonon interacting with acoustic phonons, which is consistent with the experimental conditions of optical phonon excitation using infrared laser.[15] The optical phonon is usually created at the one end of the molecule like in 2D IR measurements,[15] where the end group (usually azido group) is excited, for example, by an infrared laser pulse and then initiate the wavepacket that propagates toward the opposite end. The width of the wavepacket is determined by the specific of excitation and can be quite narrow as discussed in earlier work.[21] In the present work, this narrow wavepacket is approximately modeled using the periodic boundary conditions and optical phonon placed into the initial state with the certain wavevector.

Below, we set up the theoretical model by first defining an optical phonon Hamiltonian that describes the optical phonons, then we define an acoustic phonon Hamiltonian for the transverse modes, and finally, we describe the coupling between them.

A. Boundary conditions and normal modes

The molecule is represented by a circular periodic chain of N identical sites (unit cells) separated by a distance a. Although real

chains are not circular, this model is still relevant since the propagation of phonon should not be sensitive to boundaries if the chain length $L = Na$ exceeds the coherence length of a pure ballistic propagation of phonons. In this regime, the boundary conditions are not significant. In the opposite regime where the transport remains ballistic at distances exceeding the molecular length, the decoherence is irrelevant. The use of periodic model simplifies numerical studies because of the quasi-wavevector conservation[28] that permits us to investigate numerically longer chains than with other boundary conditions and to avoid the complicated consideration of the wavepacket.

Normal modes of the periodic chain for any specific band can be enumerated by integer numbers n and characterized by a wavevector

$$k = \frac{2\pi n}{L},\ L = Na,\ n = \begin{cases} -\frac{N-1}{2}, \dots \frac{N-1}{2} & \text{if } N \text{ is odd}, \\ -\frac{N}{2}+1, \dots \frac{N}{2} & \text{if } N \text{ is even}. \end{cases} \quad (1)$$

Wavevectors are chosen to make phonon states periodic since their site dependence is determined by the exponent e^{ikx}, where x is the position of the site.

B. Optical phonons

We describe the optical phonon band using a standard Hamiltonian,[17]

$$\widehat{H}_{\text{opt}} = \sum_k \hbar\omega_{\text{opt}}(k)\widehat{a}_k^\dagger \widehat{a}_k, \quad (2)$$

where the bosonic operators $\widehat{a}_k$ ($\widehat{a}_k^\dagger$) represent annihilation (creation) operators of optical phonons characterized by the wavevector k defined in Eq. (1) and $\omega_{\text{opt}}(k)$ stands for the wavevector dependent phonon frequency. It is a periodic function of the wavevector with the period $2\pi/a$, and it is an even function, because of the time reversal invariance. We model the phonon spectrum with the simplest periodic function,

$$\omega_{\text{opt}}(k) = \omega_0 + \frac{\Delta_{\text{opt}}(1-\cos(ka))}{2}, \quad (3)$$

corresponding to the nearest neighbor interaction of site vibrations in the coordinate representation.[17] Here, ω_0 is the optical phonon bandgap $0 < \Delta_{\text{opt}} \ll \omega_0$ and Δ_{opt} is the bandwidth. In all calculations below, we assume $\omega_0 = 1000\ \text{cm}^{-1}$ and $\Delta_{\text{opt}} = 100\ \text{cm}^{-1}$ similarly to Ref. 17, which is quite consistent with optical phonon energy band properties for organic polymer chains.[31] Generalization to a more complicated spectrum is straightforward.

The optical phonon transport is defined by the phonon current that reads

$$\widehat{J} = \sum_k v_{\text{opt}}(k)\widehat{a}_k^\dagger \widehat{a}_k, \quad v_{\text{opt}}(k) = \frac{\partial\omega_{\text{opt}}}{\partial k} = \frac{a\Delta}{2}\sin(ka), \quad (4)$$

where $v_{\text{opt}}(k)$ is velocity of the phonon with the given wavevector k, which coincides with the group velocity for the same wavevector. This average current is evaluated numerically in Sec. IV to characterize the energy transport and its suppression by decoherence.

C. Transverse acoustic phonons

Transverse acoustic phonons, i.e., collective bending modes, are discarded in most considerations of thermal energy transport possibly because they possess a vanishing group velocity $v(q) \propto q$ in the long wavelength limit,[23,26,32–35] while longitudinal phonons possess a constant speed of sound. However, transverse acoustic phonons provide a more significant source of dissipation as a sub-Ohmic bath,[26] so they can be significant for optical phonon decoherence.

The Hamiltonian of transverse acoustic phonons for each band $\mu = 1, 2$ corresponding to two possible directions of transverse displacement can be expressed as

$$\widehat{H}_{\text{tr}} = \sum_{q,\mu} \hbar\omega_{\text{tr}\mu}(q)\widehat{b}_{q\mu}^\dagger \widehat{b}_{q\mu}, \quad (5)$$

where bosonic operators $\widehat{b}_{q\mu}$ ($\widehat{b}_{q\mu}^\dagger$) represent the annihilation (creation) operators of transverse phonons within the normal modes characterized by the operator subscript indices.

Transverse phonon frequencies are periodic functions of the wavevector, approaching 0 for $k \to 0$. We consider the simplest possible model for their spectrum, that is similar to the one for optical phonons [Eq. (3)] but with the zero bandgap,

$$\omega_{\text{tr}\mu}(q) = \frac{\Delta_{\text{tr}\mu}(1-\cos(qa))}{2}, \quad (6)$$

where $\Delta_{\text{tr}\mu}$ is the transverse acoustic phonon bandwidth for the specific branch $\mu = 1$ or 2. The spectrum in Eq. (6) is originated from a potential energy determined by local "bendings" $\widehat{\epsilon}_{n,\mu} = (\widehat{u}_{n-1,\mu} - 2\widehat{u}_{n,\mu} + \widehat{u}_{n+1,\mu})/a$ in the form $U_{bend}^{\mu} = \frac{A_\mu}{2}\sum_n \widehat{\epsilon}_{n,\mu}^2$, where $\widehat{u}_{n,\mu}$ is the displacement operator of the site n in the direction μ, the parameter A_μ is defined as $A_\mu = Ma^2\Delta_{\text{tr}\mu}^2/4$, and M is the mass of the elementary cell. The displacement operator $\widehat{u}_{n,\mu}$ for the site n is connected to the bosonic operators $\widehat{b}_{q\mu}$ as[36]

$$\widehat{u}_{n,\mu} = \frac{1}{\sqrt{N}}\sum_q \sqrt{\frac{\hbar}{2M\omega_{\text{tr}\mu}(q)}}e^{iqna}\left(\widehat{b}_{-q\mu} + \widehat{b}_{q\mu}^\dagger\right). \quad (7)$$

If the molecule is immersed into a solvent, then the acoustic phonon spectrum might acquire a small gap, because the solvent violates the translational invariance[36] for atoms belonging to the molecule. Since this gap is determined by the interaction with the environment that is much weaker compared to intramolecular interaction, we ignore it.

We limit further consideration to the interaction of optical phonons with a single transverse acoustic band, since the addition of the second band will not modify results qualitatively, while the generalization to two bands is quite straightforward. Consequently, we skip the earlier introduced index μ everywhere for the single transverse band considered below.

Similarly to Ref. 17, the relationship of acoustic and optical phonon bandwidths is a critically important parameter. We introduce it as a separate ratio parameter r defined as

$$r = \frac{\Delta_{\text{tr}}}{\Delta_{\text{opt}}}. \quad (8)$$

Acoustic bands are wider than optical bands since they are determined by direct atomic interactions through covalent bonds, so usually, one has $r > 1$ (see, e.g., Ref. 24).

D. Anharmonic interaction of optical phonons with transverse phonons

Anharmonic interactions are weaker compared to harmonic ones by the ratio of the typical vibration amplitude to the interatomic distance represented by the dimensionless parameter $\eta \sim 0.1$ [see Ref. 17 and Eq. (11)]. The effective strength of the pth order anharmonic interaction is expressed by the parameter η^{p-2} since harmonic interaction emerges in the second order with respect to the parameter η.

As in earlier work,[17,37] we only include cubic couplings, these being the largest. We further restrict these contributions to include only those terms that couple the nearly degenerate states describing the absorption or emission of transverse photons by optical photons. Specifically, we write

$$\widehat{V}_{\rm anh} = \frac{\hbar}{\sqrt{N}} \sum_{k,q}{}' \left[V(q,k) \widehat{a}_k^\dagger \widehat{a}_{k+q} \widehat{b}_q^\dagger + H.C. \right], \tag{9}$$

where $\sum'$ means that we use the periodic extension of the wavevector $k+q$ replacing it with $k+q \pm 2\pi/a$ if it is outside the domain of the wavevectors $(-\pi/a, \pi/a)$. $V(k,q)$ is the interaction constant of optical and transverse acoustic phonons; one has $V(q,k) \propto q$ for $q \to 0$.[26]

For future consideration, we take the interaction in Eq. (9) in the form corresponding to the nearest neighbor interactions within the coordinate representation,

$$\widehat{V}_{\rm loc} = \frac{\hbar V_0}{a} \sum_{i=1}^{N} \widehat{a}_i^\dagger \widehat{a}_i (\widehat{u}_{i+1} - 2\widehat{u}_i + \widehat{u}_{i-1}), \tag{10}$$

where $V_0 \sim \Delta_{\rm opt,tr}$ is the interaction constant and operators $\widehat{u}_i$ stand for the transverse displacements at the site i [Eq. (7)] interacting with the local densities of optical phonons $(\widehat{a}_i^\dagger \widehat{a}_i)$. For this specific model, the interaction constants $V(q,k)$ in Eq. (9) can be expressed as

$$V(q,k) = 2V_3 \left| \sin\left(\frac{qa}{2}\right) \right|, \quad V_3 = \eta V_0, \quad \eta = \sqrt{\frac{2\hbar}{Ma^2 \Delta_{\rm tr}}} \sim 0.1. \tag{11}$$

This definition is used in all considerations below. The coupling constant V_3 represents a characteristic strength of anharmonic interactions that should be smaller compared to the harmonic interactions by the small factor η.

E. Full Hamiltonian

The full Hamiltonian of the system includes Hamiltonians of optical [Eq. (2)] and transverse [Eq. (5)] phonons and their interaction [Eq. (9)] as rewritten as follows for reader convenience:

$$\widehat{H}_{\rm tot} = \sum_k \hbar \left(\omega_0 + \Delta_{\rm opt} \frac{1 - \cos(ka)}{2} \right) \widehat{a}_k^\dagger \widehat{a}_k + \sum_q \hbar \Delta_{\rm tr} \frac{1 - \cos(qa)}{2} \widehat{b}_q^\dagger \widehat{b}_q + \frac{2\hbar V_3}{\sqrt{N}} \sum_{q,k}{}' \left[\sin(qa/2) \widehat{a}_k^\dagger \widehat{a}_{k+q} \widehat{b}_q^\dagger + H.C. \right], \tag{12}$$

using Eqs. (3) and (6) for optical and transverse phonon frequencies, respectively, and Eq. (11) for anharmonic interactions.

F. Higher order anharmonic interactions

The model under consideration includes only the third order anharmonic interactions [Eq. (9)]. However, higher order interactions are generated by the third order interactions in a perturbation theory.[28] Therefore, all decoherence channels originated from higher order interactions are present within our model [Eq. (12)] in the proper order in the small parameter η [Eq. (11)]. For future consideration, we need the fourth order interaction, because it is responsible for the optical phonon backscattering in the case of a narrow optical phonon band, $r > 1$, where r is the ratio of transverse to optical phonon bandwidths [Eq. (8)]. The fourth order interaction is very important for the regime $r > 1$ since in this regime, the third order interaction leads to only forward scattering and cannot overturn propagating optical phonon (see Sec. III A). Indeed, it contains the resonant scattering of optical and acoustic phonons with opposite momentum expressed, for example, by the terms $a_{-k}^\dagger b_k^\dagger a_k b_{-k}$ overturning the optical phonon current, independent of the bandwidth ratio r. Higher order anharmonic interactions generated in higher orders of perturbation theory also lead to optical phonon backscattering. They are less important compared to the fourth order interactions in the ratio of the atomic displacement to the interatomic distance [Eq. (11)]. The perturbation theory developed below is not applicable to the regime of the small bandwidth ratio $r < 1$ as shown below in Sec. III. In that case, backscattering can be completed by the third order processes leading to much faster phonon transitions.

We derive the fourth order interaction using the degenerate Van Vleck perturbation theory,[38,39] which is technically equivalent to the Schrieffer–Wolff transformation[40] eliminating off-resonant third order anharmonic interactions to generate the resonant interaction in the fourth order. For the system Hamiltonian separated into the harmonic part $\widehat{H}_0$ and the perturbation $\widehat{V}$ (anharmonic interactions), we introduce the unitary transformation of the Hamiltonian as $\widehat{H} \to e^{\widehat{S}} \widehat{H} e^{-\widehat{S}}$ with the anti-Hermitian operator $\widehat{S}$ defined as $[\widehat{S}, \widehat{H}_0] = -\widehat{V}$. Then, the expansion of the exponents in the power series in $\widehat{S}$ results in a disappearance of the off-resonant part of the perturbation $\widehat{V}$ (the perturbation expansion is not applicable to a resonant part) with a simultaneous generation of the fourth order interaction in the form[40]

$$\widehat{H} \approx \widehat{H}_0 + \widehat{V}_{\rm res} + \frac{1}{2} [\widehat{S}, \widehat{V}_{\rm offres}], \tag{13}$$

where the anharmonic interaction $\widehat{V}$ is split into resonant $\widehat{V}_{\rm res}$ and off-resonant $\widehat{V}_{\rm offres}$ parts.

For the specific Hamiltonian in Eq. (12), one can express the matrix $\widehat{S}$ in the form

$$\widehat{S} = -\frac{1}{\sqrt{N}} \sum_{q,k}{}' \left[V(q,k) \frac{\widehat{a}_k^\dagger \widehat{a}_{k+q} \widehat{b}_q^\dagger}{\omega_{\rm opt}(k) - \omega_{\rm opt}(k+q) - \omega_{\rm tr}(q)} - H.C. \right]. \tag{14}$$

The modified summation $\sum'$ means omitting resonant terms with $|\omega_{\rm opt}(k) - \omega_{\rm opt}(k+q) - \omega_{\rm tr}(q)| \le \eta^2 \Delta_{\rm opt}$ to make both the Schrieffer–Wolff perturbation theory and the Fermi golden rule for the third order anharmonic interaction applicable and using the

proper definition of the wavevector sum $k+q$ shifted by $\pm 2\pi/a$ if necessary, to match the wavevector domain $(-\pi/a, \pi/a)$ [Eq. (1)].

The induced fourth order anharmonic interaction can be evaluated using Eq. (13) as

$$\widehat{V}_4 = -\frac{4\hbar V_3^2}{N\Delta_{\rm opt}} \sum_{k,q,p}{}' a_k^\dagger b_q^\dagger a_{k-p} b_{q+p} \times \left[\frac{\sin\left(\frac{q+p}{2}\right)^2 \cos\left(k-\frac{p}{2}\right)}{\left(r\sin\left(\frac{q}{2}\right) - \sin\left(k+\frac{q}{2}\right)\right)\left(r\sin\left(\frac{q}{2}\right) - \sin\left(k-p-\frac{q}{2}\right)\right)} + \frac{\sin\left(\frac{q}{2}\right)^2 \cos\left(k-\frac{p}{2}\right)}{\left(r\sin\left(\frac{q+p}{2}\right) - \sin\left(k+\frac{q-p}{2}\right)\right)\left(r\sin\left(\frac{q+p}{2}\right) - \sin\left(k-\frac{p+q}{2}\right)\right)} \right]. \quad (15)$$

Remember that r is the transverse to optical phonon bandwidth ratio [Eq. (8)].

Equation (15) contains denominators that can approach zero. For $r > 1$, there are no zero denominator for the fourth order resonant backscattering processes since the fourth order process is composed of two virtual third order processes, conserving the wavevector. These processes cannot both conserve energy as needed for a zero denominator since at least one of them must include resonant optical phonon backscattering accompanied by absorption or emission of an acoustic phonon, which is forbidden for $r > 1$ (see Sec. III). The resonant terms associated with the forward scattering lead to the broadening of optical phonon energy levels. This broadening can affect forward and backscattering rates for large anharmonic coupling, leading to the failure of the Fermi golden rule as discussed in Sec. III C.

In addition to the induced fourth order anharmonic interaction [Eq. (13)], there exists the interaction emerging similarly to the third order interaction in Eq. (9). This interaction will be also of the second order in the parameter η in Eq. (11) as that in Eq. (15), so it gives the effect comparable to that of the induced interaction. Since our consideration is qualitative and does not target the specific molecule, we can neglect that interaction.

III. OPTICAL PHONON TRANSITIONS INDUCED BY ANHARMONIC INTERACTIONS

The anharmonic interactions of an optical phonon with transverse acoustic phonons [Eq. (11)] can lead to transitions of this optical phonon between different states emerging in the continuous spectrum for sufficiently long chains ($N \gg 1$). Such transitions affect a current associated with this phonon. In particular, transitions accompanied by the overturn of the phonon velocity lead to ballistic transport breakdown with its further replacement with the diffusive transport.

Below, we examine the phonon transitions permitted by the energy and momentum (wavevector) conservation, estimate their rates using the Fermi golden rule, and consider qualitatively other regimes, not handled by the Fermi golden rule. In these regimes, an anharmonic interaction is either too strong to be treated as a perturbation or too weak to neglect the discreteness of the system at a finite number of sites N. All regimes are revealed in the numerical studies reported in Sec. IV.

A. Emission and absorption

1. Energy and momentum conservation

The emission or absorption of transverse phonon in a periodic chain emerges with energy and quasi-momentum (wavevector) conservation. If initially the optical phonon has a wavevector k and after emission it acquires the wavevector k', then the wavevector of the emitted transverse phonon is equal to $q = k - k'$ with the accuracy to the inverse lattice period $2\pi/a$. For absorption, the wavevector of the absorbed phonon is given by $q = k' - k$. In either case, the frequency of the emitted or absorbed phonon satisfies the energy conservation law in the following form:

$$\begin{aligned} \omega_{\rm opt}(k) - \omega_{\rm opt}(k') &= \omega_{\rm tr}(k-k') \quad \text{(absorption)}, \\ \omega_{\rm opt}(k') - \omega_{\rm opt}(k) &= \omega_{\rm tr}(k'-k) \quad \text{(emission)}. \end{aligned} \quad (16)$$

These equations are not solvable for the emission or absorption of longitudinal phonons possessing sound velocity exceeding the maximum group velocity of optical phonons in accord with Cherenkov's emission criterion of Ref. 17. This is not the case for the transverse phonons as illustrated in Fig. 1 for the modeling phonon spectra [Eqs. (3) and (6)]. The solution always exists because the group velocity of transverse phonons approaches zero at small wavevectors violating Cherenkov's constraint.

Yet the graphical solutions of Eq. (16), expressing the energy conservation law, are different for different ratios r of optical and acoustic phonon bandwidths, as illustrated in Fig. 1 for $r = 1/3$ and $r = 3$. Namely, for $r < 1$, initial and final wavevectors are of opposite signs, so the emission or absorption is accompanied by the overturn of the optical phonon propagation direction, i.e., backscattering,

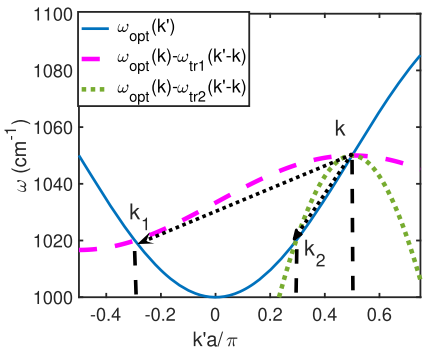

FIG. 1. Graphical solution for the emission of transverse phonon [Eq. (17)]. The initial optical phonon wavevector is k, and the final one is k'. The dashed (magenta) and dotted (green) lines are defined as $y(k') = \omega_{\rm opt}(k) - \omega_{\rm tr}(k-k')$ and used to find the solution of Eq. (16) for the emitted phonon wavevector k' as the graph intersection $y(k') = \omega_{\rm opt}(k')$ for narrow ($\Delta_{\rm tr} = \Delta_{\rm opt}/3$) or wide ($\Delta_{\rm tr} = 3\Delta_{\rm opt}$) transverse phonon bands, respectively. The black arrows illustrate wavevector modifications after transverse phonon emission.

while in the opposite case $r > 1$, initial and final wavevectors are of the same signs as for scattering forward. This observation is in full accord with the analytical solution of Eq. (16) for the modeling spectra in Eqs. (3) and (6), where we obtained (remember, $r = \Delta_{tr}/\Delta_{opt}$)

$$q = \frac{2}{a}\tan^{-1}\left(\frac{\sin(ka)}{r+\cos(ka)}\right) \quad \text{(emission)},$$
$$q = \frac{2}{a}\tan^{-1}\left(\frac{\sin(ka)}{-r+\cos(ka)}\right) \quad \text{(absorption)}. \tag{17}$$

It is clear from both solutions [Eq. (17)] that the unity ratio $r = 1$ serves as the crossover regime $q = k$ for emission or $q = \pi/a - k$ for absorption, while for $r > 1$ and $k > 0$, one has $0 < q < k$ for emission and $0 < q < \pi/a - k$ for absorption, leaving the wavevector k' positive. For $r < 1$, it inevitably changes direction after both absorption and emission. These conclusions remain valid for arbitrary phonon spectra at sufficiently large ($r \gg 1$) or small ($r \ll 1$) ratios since for $r \gg 1$, the only small wavevector change leaves phonon energy within the optical band, while for $r \ll 1$, one has $q \approx 2k$ since the narrow band reflects optical phonon backward almost statically (see also Fig. 1).

Based on this consideration, we can conclude that the emission and absorption of transverse phonons occur differently depending on the ratio r of transverse acoustic to optical phonon bandwidths. If $r > 1$, then the change of the wavevector of optical phonon during emission or absorption is smaller than the wavevector itself. Consequently, single phonon absorption or emission cannot overturn the direction of the phonon propagation. Backscattering requires higher order anharmonic processes considered in Sec. III B. These processes can be orders of magnitude slower than single phonon absorption or emission as it is demonstrated in the numerical simulations reported in Sec. IV. Consequently, a unidirectional propagation of vibrational energy lasts for a while. Experimentally, this regime is seen quite similarly to a ballistic transport since after a phonon equilibration among the states with a certain wavevector direction, the transport speed should approach a constant value given by its proper average over those states.

In the opposite regime of a smaller acoustic phonon bandwidth, single phonon absorption or emission is accompanied by the change of the direction of phonon propagation. Consequently, ballistic transport breaks down after a single or few absorption or emission events, which is consistent with our numerical studies reported in Sec. IV.

2. Absorption and emission rates

Consider the optical phonon having the wavevector k. Due to its anharmonic interaction [Eq. (9)], it can emit or absorb an acoustic phonon with the wavevector q [Eq. (17)] getting to the new state within the same band, characterized by the wavevectors $k \mp q$ due to the quasi-momentum conservation. In a first non-vanishing order in a weak anharmonic interaction, the rate of this transition is given by the Fermi golden rule. According to this rule, emission and absorption rates (W_{em} and W_{abs}) can be expressed as (cf. Refs. 17 and 41)

$$W_{em} = a\int_{-\pi/a}^{\pi/a} dk'\, V(k-k',k)^2 \delta\big(\omega_{opt}(k) - \omega_{opt}(k') - \omega_{tr}(k-k')\big)(1+\nu(k-k')),$$
$$W_{abs} = a\int_{-\pi/a}^{\pi/a} dk' V(k'-k,k)^2 \delta\big(\omega_{opt}(k) - \omega_{opt}(k') + \omega_{tr}(k-k')\big)\nu(k-k'),$$
$$\nu(q) = \frac{1}{e^{\frac{\hbar\omega_{tr}(q)}{k_B T}} - 1}, \tag{18}$$

where $\nu(q)$ represents the average number of transverse phonons with the wavevector q, defined in Eq. (17).

Using the specific phonon spectra and interactions, defined by Eqs. (3), (6), and (11), we evaluate the integral in Eq. (18) as

$$W_{em} = 8\frac{V_3^2}{\Delta_{opt}}(1+\nu(q))\frac{\sin(ka)}{r^2+2r\cos(ka)+1},$$
$$W_{abs} = 8\frac{V_3^2}{\Delta_{opt}}\nu(q)\frac{\sin(ka)}{r^2-2r\cos(ka)+1}. \tag{19}$$

At high temperatures where population numbers can be replaced with their classical expressions [$\nu(x) = k_B T/(\hbar\omega_{tr}(x))$ and $\nu(x) \gg 1$], we get

$$W_{em} = 8\frac{V_3^2}{\Delta_{opt}}\frac{k_B T}{\hbar\Delta_{tr}\sin(ka)},\quad W_{abs} = 8\frac{V_/3^2}{\Delta_{opt}}\frac{k_B T}{\hbar\Delta_{tr}\sin(ka)},$$
$$W_{tot} = W_{abs} + W_{em} = 16\frac{V_3^2}{\Delta_{opt}}\frac{k_B T}{\hbar\Delta_{tr}\sin(ka)}, \tag{20}$$

where W_{tot} represents the total decay rate of the optical phonon.

The lifetime T_{rel} of the optical phonon in the given quantum state can be estimated as the inverse total decay rate,

$$T_{rel} = \frac{1}{W_{tot}}. \tag{21}$$

The inverse lifetime defines the inelastic width of the energy level as $\hbar/T_{rel}$.

B. Backscattering for a large bandwidth ratio $r > 1$

1. Backscattering at high temperature. Fourth order processes

At a large bandwidth ratio $r > 1$, backscattering can arise from the phonon scattering expressed by the fourth order anharmonic interaction [Eq. (15)], which is the next anharmonic correction to the third order interaction considered above. There are no constraints for the energy conservation for phonon scattering as can be illustrated for instance by the resonant backscattering of optical and acoustic phonons with opposite wavevectors resulting in their wavevector exchange. Such processes require the presence of excited acoustic phonons that is possible if the thermal energy $k_B T$ is at least comparable to or larger than the transverse bandwidth $\hbar\Delta_{tr}$. In the opposite case of low temperature $k_B T \ll \hbar\Delta_{tr}$, multiphonon emission is needed for the optical phonon backscattering as shown in Sec. III B 2.

The backscattering rate can be estimated using the Fermi golden rule with the interaction in Eq. (13) as a perturbation. Because of the large number of scattering outcomes, we do not attempt to calculate a specific relaxation rate, but instead consider its dependence on the anharmonic coupling V_3, bandwidth ratio r assuming $r > 1$, and temperature T in a thermodynamic limit of a sufficiently long chain, where the continuum approach is applicable (see the discussion of discreteness in Sec. III C 2).

At high temperatures $k_B T > \hbar\Delta_{tr}$, one can estimate the coupling matrix element for the processes relevant for the optical phonon overturn in Eq. (13) as $\hbar V_4 = \hbar V_3^2 k_B T/(r^3 \Delta_{opt}^2)$. The transition rate produced by the Fermi golden rule can then be estimated as

$$W_4 \sim \frac{V_4^2}{\Delta_{tr}} = C\frac{V_3^4 (k_B T/\hbar)^2}{r^7 \Delta_{opt}^5}, \quad C \approx 3 \cdot 10^4, \tag{22}$$

where C is the dimensionless proportionality constant determined numerically in Sec. IV B 4. Equation (22) is approximately consistent with the numerical results for the phonon current relaxation rate reported in Sec. IV, where the large magnitude of the proportionality constant C in Eq. (22) is explained on a semiquantitative level. The fourth order anharmonic interaction with longitudinal phonons should result in a relaxation rate behaving similar to Eq. (22) since longitudinal and transverse branches are weakly distinguishable for a large phonon wavevector $k, q \sim \pi/a$ relevant for that regime.

2. Backscattering at low temperature: Multiphonon emission

If the temperature is very low so that there are no acoustic phonons capable of scattering initially excited optical phonon backward, then the only remaining option for the optical phonon overturn is multiphonon emission. Such a process is forbidden for longitudinal acoustic phonons possessing the velocity exceeding that of optical phonons,[17] but it is allowed for transverse acoustic phonons even for $r \gg 1$ as shown below.

As an illustration, consider the overturn of the optical phonon with the wavevector k by means of the emission of n transverse phonons with wavevectors $q_1, q_2, \ldots, q_n$ and total wavevector $\sum_{i=1}^n q_i = k$, which is the minimum wavevector change corresponding to the overturn that should take place simultaneously with the frequency change $\sum_{i=1}^n \omega_{tr}(q_i) = (\omega_{opt}(q) - \omega_{opt}(0))$ due to energy conservation law. The most efficient emission takes place at the minimum number n of emitted transverse phonons since the emission rate decreases exponentially as η^{2n} with increasing n [see Eq. (11) for the definition of η].

It can be shown rigorously for our specific phonon spectrum [Eq. (6)] and generalized to any monotonic function $\omega_{tr}(q)$ that the optimum emission regime is realized for all identical emitted transverse phonons with wavevectors $q_i = k/n$. Assuming a large number of phonons, $n \gg 1$, which is valid for $r \gg 1$, we can approximate the total emitted energy as $\hbar\Delta_{tr} a^2 k^2/(4n)$, and we estimate the minimum number of emitted phonons needed for the overturn as

$$n = \eta_{ph} r, \quad \eta_{ph} = \frac{k^2 a^2}{4\sin(ka/2)^2}. \tag{23}$$

Thus, in our model, the number of transverse phonons needed to be emitted is proportional to the bandwidth ratio r with the proportionality coefficient η_{ph} ranging from 1 to $\pi^2/4 \approx 2.5$. The multiphonon emission rate W_{mult} is proportional to the squared coupling constant for the n phonon process. Consequently, we expect that

$$W_{mult} \propto \eta^{2\eta_{ph} r}, \tag{24}$$

where $\eta \sim 0.1$ [Eq. (11)]. An additional dependence on the number of emitted phonons can be originated from the wavevector dependence of the n-phonon interaction constant. We do not investigate this dependence in detail, because we were not able to reproduce this regime numerically as reported in Sec. IV A, so it cannot be compared to any experimental or numerical observation.

C. Regimes of Fermi golden rule failure

Here, we consider the regimes that cannot be characterized by Fermi golden rule rates. These considerations are needed for understanding dynamics observed in numerical simulations reported in Sec. IV for very large or very small anharmonic interactions.

The Fermi golden rule fails at very large anharmonic interactions V_3 in Eq. (11), where the perturbation theory is no more applicable, and at very small anharmonic interactions, where the discreteness of the phonon spectrum becomes important. Below, we address both regimes.

1. Strong anharmonic coupling

Consider the evolution of the initial harmonic state a with certain wavevectors of all phonons. The population $P_a(t)$ of this state decreases with time due to anharmonic interactions. At short times, it decreases as $P_a(t) = 1 - W_*^2 t^2$, where $W_* = V_*/\hbar$, and $V_* = \sqrt{\sum_{b\neq a} V_{ab}^2}$, where V_{ab} is the off-diagonal matrix element of anharmonic interaction coupling harmonic states a with any other harmonic state b possessing harmonic energies E_a and E_b, respectively. For a weak anharmonic interaction, where the Fermi golden rule is applicable, this decay slows down at times much shorter than the effective minimum relaxation time $T_* \approx 1/W_*$, since the squared time dependence for each specific state b saturates at time $t \sim \hbar/|E_a - E_b|$. For a strong interaction, the maximum rate W_* gives a reasonable estimate for the relaxation rate consistent with the numerical results of Sec. IV.

For future comparisons with numerical results, we report the maximum relaxation rate W_* and its asymptotic behaviors at high and low temperatures evaluated for the anharmonic interaction Eq. (11) as

$$W_* = \sqrt{\frac{1}{N}\sum_q 4V_3^2 \sin^2(qa/2)\left(1 + \frac{2}{e^{\frac{\hbar\omega_{tr}(q)}{k_B T}} - 1}\right)} = \begin{cases} \sqrt{2}V_3, & k_B T \ll \Delta_{tr} \\ 4\sqrt{2}V_3\sqrt{\dfrac{k_B T}{\Delta_{tr}}}, & k_B T \gg \Delta_{tr}. \end{cases} \tag{25}$$

2. Weak anharmonic coupling: Effect of discreteness

Fermi's golden rule is applicable to the continuous spectrum in the infinite chain limit. The spectrum can be treated as continuous if the energy uncertainty associated with the specific state decay

rate Eq. (19) defined as $\hbar W_{\rm tot}$ exceeds the interlevel splitting given by $\Delta E \approx (2\pi\hbar/L)\ \max(|\partial\omega_{\rm tr}(k)/\partial k|, |d\omega_{\rm opt}(k)/dk|)$, where L is the chain length. Comparing two energies to each other, we derived the constraint on the strength of anharmonic interaction V_3 needed for the Fermi golden rule to be applicable, which can be expressed as

$$V_3 > \max(1,\sqrt{r})\frac{\Delta_{\rm opt}}{\sqrt{N}}\begin{cases}\sqrt{\dfrac{\pi(1+2r\cos(ka)+r^2)}{8}}, & k_{\rm B}T \ll \hbar\Delta_{\rm tr},\\ \dfrac{\sin(ka)}{4}\sqrt{\dfrac{\pi r\hbar\Delta_{\rm opt}}{k_{\rm B}T}}, & k_{\rm B}T \gg \hbar\Delta_{\rm tr}.\end{cases} \tag{26}$$

If Eq. (26) is not satisfied, then the optical phonon state time evolution will depend on the temperature and the molecular length. At low temperatures and reasonably short chains $N \sim 10$, the non-ergodic behavior can emerge[5,28,42,43] similarly to that found in earlier work,[17] where the interaction of optical phonons with longitudinal acoustic phonons was considered. In the non-ergodic or many-body localized regime,[5,28] optical phonon current in a periodic chain will never relax to zero staying close to its initial value, except for the states with the total wavevector 0 or π/a where it disappears in average due to the inversion symmetry. Yet in the non-ergodic regime, the current does not relax to zero but coherently oscillates switching between positive and negative values.

There is a greater chance to observe the localized regime for a larger bandwidth ratio r since the critical strength of anharmonic coupling separating discrete and quasi-continuous regimes grows with r as $r^{3/2}$. At high temperatures, the ergodic behavior should be restored due to phonon scattering. All these expectations are reasonably consistent with the results of numerical simulations reported in Sec. IV.

IV. NUMERICAL STUDIES

Here, we numerically model our Hamiltonian equation (12) for optical phonon transport in order to test the validity of the analytical results described in Sec. III. We study how the transport in periodic atomic chains is affected by the interaction with transverse acoustic phonons using fully quantum mechanical or semiclassical approaches for periodic atomic chains. The quantum mechanical treatment reported in Sec. IV A is developed similarly to earlier work[17] considering longitudinal acoustic phonons. It is limited to relatively short chains and small total energies (very low temperatures) because of the exponential increase in the number of significant quantum states with energy and number of sites N, which prohibits an accurate numerical diagonalization for longer chains. The second approach (Sec. IV B) treats acoustic phonons and their interaction with the optical phonon classically, which permits us to characterize large systems at high temperatures, where this consideration is reasonably justified.

A. Quantum mechanical treatment

The full quantum-mechanical treatment of optical phonon transport is quite similar to earlier work[17] (see also Ref. 28). Exact diagonalization of the system Hamiltonian equation (12) is not possible since the basis of its possible states is infinitely large. However, for the states with relatively small energies, we can limit our consideration to a number of acoustic phonons not exceeding a certain maximum number $n_{\rm max}$ and perform full diagonalization with that limited basis.[17,28] Our approximation can be validated considering the dependence of certain parameters of interest on the number $n_{\rm max}$. In most of the calculations, we investigated the time evolution of the probability $P_n(t)$ to find the excited optical phonon in its initial state with a certain wavevector $k = 2\pi n/L$ and we used its infinite time limit $P_n(\infty)$ as a convergence control parameter.

The calculations reported below are performed for a periodic chain of $N = 12$ sites and the anharmonic interaction strength $V_3 \le 0.5\Delta_{\rm opt}$. In this specific case, a good convergence for probabilities $P_n(\infty)$ is obtained for $n_{\rm max} = 6$, which corresponds to the basis of 12 376 states. The difference of the results for $n_{\rm max} = 5$ and $n_{\rm max} = 6$ is always less than few percents, and their difference for $n_{\rm max} = 6$ and $n_{\rm max} = 7$ is less than 1%. Therefore, we believe that our method gives a good approach to the actual quantum evolution of the system.

We investigate the relaxation of the current for the initially excited optical phonon with the wavevector $k = 2\pi n/(aN)$, Eq. (1). The state with number $n = N/4 = 3$ is chosen because it is located in the middle of the band and possesses a maximum phonon velocity $v(k) = \Delta_{\rm opt}\sin(ka)/2$ realized at $ka = \pi/2$ [Eq. (4)]. The results for other initial wavevectors are quite similar, except for $n = 0$ where no relaxation is seen for $V < 0.5\Delta_{\rm opt}$ for any considered bandwidth ratios because it is the lowest energy optical phonon state having no decay channels. Since the observed dependence on the initial wavevector is quite similar to that reported in Ref. 17, we do not show the results of calculations for $n \neq 3$. We evaluate the current following its definition in Eq. (4) using the optical phonon time-dependent density matrix ρ_{kk} as $J = \sum_k \rho_{kk}\partial\omega_{\rm opt}(k)/\partial k$, where the summation is made over all optical phonon normal modes enumerated by their wavevectors k.

We investigated two different initial states, including (A) the initial state with a single excited optical phonon with the wavevector $k = 2\pi n/L$ and (B) the two-phonon initial state with a single excited optical phonon with the same wavevector k and a single acoustic phonon with the wavevector $-k$. Case (A) earlier used in Ref. 17 is targeted to examine the relaxation due to the emission of acoustic phonons, while in case (B), we also investigate the effect of resonant backscattering on the optical phonon current for a large bandwidth ratio $r > 1$. The more complicated initial conditions are briefly discussed in the end of the present section.

Our initial conditions correspond to zero temperature in a thermodynamic limit of an infinite system size with $T \propto 1/N$. The full quantum mechanical consideration of a finite temperature is problematic because of the exponential increase in the number of relevant states with the temperature.

1. Single excited optical phonon

The time evolution of the optical phonon current for the initial state containing only one excited optical phonon with the wavevector $k = \pi/(2a)$ $(N = 12)$ is shown in Fig. 2(a) for four different bandwidth ratios r. We choose the maximum coupling strength $V_3 = 0.2\Delta_{\rm opt}$, where the perturbation theory with respect to anharmonic interaction is still applicable. Infinite time limits of current shown by the dashed lines are evaluated averaging the current over time, which sets all oscillating contributions to zero as in Refs. 17 and 44.

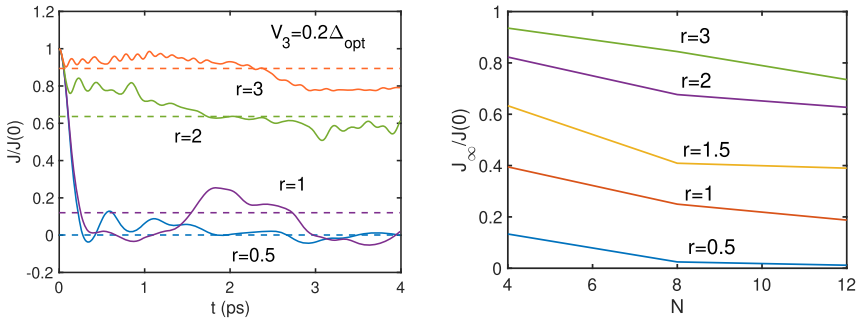

(a) (b)

FIG. 2. Time dependence of currents $J/J(0)$ (a) and size dependence of time averaged currents $J_\infty/J(0)$ (b) for different ratios r of transverse acoustic and optical bandwidths. $J(0)$ stands for the current at time $t = 0$.

The observed evolution of currents for bandwidths $r \le 1$ and $r > 1$ is clearly different. For $r \le 1$, the current rapidly decreases to the small value compared to the initial current $I(0)$, while for $r = 2$ and 3, it changes weakly compared to its initial value. We interpret this difference as the separation between ergodic ($r = 0.5$) and non-ergodic ($r = 2$ and 3) regimes. In the ergodic regime, averaging over time and over realizations should give identical results. This definition is accurate for infinite systems, while in a finite system, the difference of the results of two averagings should be small. Here, we use the approximate ergodicity criterion based on the time-averaged phonon current J_∞. Average current over realizations is zero because of the system symmetry. Consequently, for the finite system, we expect that in the ergodic regime, its time average J_∞ should be much less than its initial value $J(0)$. Consequently, for the 12 site chain, we can approximately assume that the system is ergodic if $J_\infty/J(0) < 0.1$ for the bandwidth ratio $r = 1/2$ and definitely non-ergodic if $J_\infty/J(0) > 1/2$ for $r \ge 2$. This qualitative criterion is consistent with the energy level statistics used to distinguish ergodic and non-ergodic regimes similarly to earlier work,[17] where the level statistics was reported.

According to Fig. 2(b) for considered numbers of sites $N = 4$, 8, and 12, the infinite time current J_∞ is substantially smaller than the initial current $J(0)$ for the small bandwidth ratio $r = 1/2$ where it rapidly decreases with N as it normally happens in the ergodic regime. For larger ratios $r > 2$, the infinite time current exceeds half of the initial current, which is typical for the non-ergodic behavior. However, even for $r > 1$, the ratio $J_\infty/J(0)$ also decreases with the system size so at sufficiently large $N > N_c$ where the discreteness is less significant, the ergodic behavior should emerge. The critical size N_c increases with decreasing the bandwidth ratio r in agreement with the expectations of Sec. III C 2.

We investigated the relaxation of the population of the initially excited state $P_n(t)$ in the ergodic regime $r = 1/2$ to compare relaxation times estimated using Fermi's golden rule [inverse relaxation rate $W_{\rm tot}$, Eq. (19)] with their numerical estimates. The numerical relaxation time $T_{\rm rel}$ is defined using time dependent populations $P(t)$ shown in Fig. 3(a) setting $P(T_{\rm rel}) = P_\infty + (1 - P_\infty)e^{-1}$ for $n = 3$. The numerical relaxation times are shown by diamonds in Fig. 3(b) vs anharmonic coupling strengths and compared to the Fermi golden rule estimate $W_{\rm tot}^{-1}$ [Eq. (19), dashed line] and the

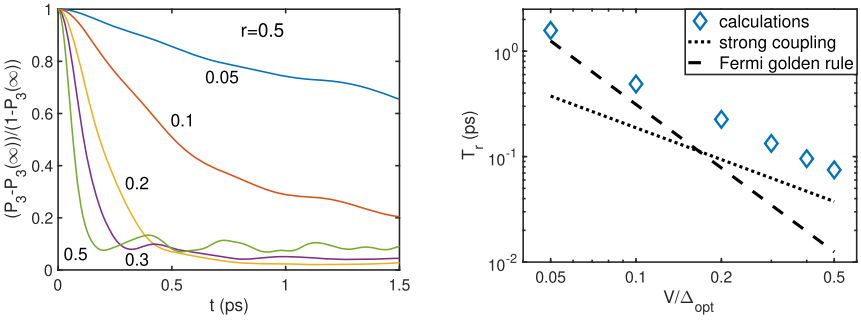

(a) (b)

FIG. 3. (a) Relaxation of the population of the optical phonon midband state for bandwidth ratio $r = 0.5$ at different strengths of anharmonic interaction. (b) Dependence of population relaxation time on the strength of anharmonic interaction shown together with the rate predicted by the Fermi golden rule (19) shown by the dashed line and characteristic minimum lifetime $1/W_*$ [Eq. (25)] shown by the dotted line.

minimum relaxation time W_*^{-1} realized for a strong anharmonic coupling [Eq. (25), dotted line]. It turns out that relaxation time switches between two regimes with increasing the coupling strength V_3 as expected. For $V_3 < 0.03\Delta_{opt}$, the relaxation is no more seen, but instead the current oscillates around its average value close to its initial value. This suggests an ergodicity breakdown emerging at $V_3 < 0.03\Delta_{opt}$ with the current evolution similar to observed behaviors for $r \geq 2$ as shown in Fig. 2(a).

Non-ergodic behaviors are caused by discreteness as discussed in Sec. III C 2. An increase in the number of sites N should most probably eliminate that behavior even for $r > 1$ in a thermodynamic limit of $N \to \infty$ due to allowed forward scattering that was lacking in the previous study.[17]

2. Two phonon initial state

To investigate the effect of a resonant two-phonon interaction onto the system dynamics, we modified the initial conditions compared to Sec. IV A 1 using an optical phonon with the wavevector $k = 2\pi n/L$ ($n = 3$, $N = 12$) and one transverse acoustic phonon with the opposite wavevector $-k$. We focus only on a nonergodic regime $r > 1$ since in the ergodic regime, the current evolution is practically the same as for the initial conditions of a single excited optical phonon reported in Sec. IV A 1.

For a two-phonon initial condition, the time-averaged optical phonon current approaches zero because of the inversion symmetry of the problem for a total wavevector equal to 0, suggesting that each eigenstate of the problem is composed of the symmetric or antisymmetric combination of pairs of states with all opposite wavevectors like $|k, -k\rangle$ and $|-k, k\rangle$ for a two-phonon state. The initial state used in Sec. IV A 1 possesses a wavevector $k = \pi/(2a)$. The conservation of the wavevector does not allow a system transition to the symmetric state with the opposite wavevector, since the difference of two state wavevectors π/a is not equal to an integer number of inverse lattice periods $2\pi/a$. Consequently, the inversion symmetry is broken and the average current differs from zero.

For a two-phonon initial condition and $r \geq 2$, the current shows nearly coherent oscillations around zero, as illustrated in Fig. 4(a) (gray line) for a bandwidth ratio $r = 4$, in a stark contrast with the time evolution for a single phonon initial condition, as shown in the same graph (magenta line). Similar oscillations were found for a wide range of anharmonic coupling strengths and bandwidth ratios $r \geq 2$.

To interpret the observed coherent oscillations, we employ the secular perturbation theory limiting our consideration to the only two resonant states $|k, -k\rangle$ (the initial state) and $|-k, k\rangle$ (the symmetric state) possessing identical harmonic energies and coupled by the fourth order anharmonic interaction $V(k, -k, -k, k) = 16\hbar V_3^2/(N\Delta_{opt}(r^2 - 1))$ [Eq. (15)]. For the given initial condition, the system coherently oscillates between these two states possessing opposite optical phonon currents with the period

$$T_{res} = \frac{2\pi\hbar}{V(k, -k, -k, k)} = \frac{2\pi(r^2 - 1)N\Delta_{opt}}{16V_3^2}. \quad (27)$$

In Fig. 4(b), we show the dependence of numerically estimated oscillation periods (symbols) on a system size and bandwidth ratios. Here, we used the maximum number of acoustic phonons equal to 5, which is justified for $N \leq 12$ but questionable for $N = 16$. Numerical estimates are consistent with the theory predictions [Eq. (27)] shown by the straight lines. Coherent oscillations of current suggest a non-ergodic behavior in spite of average current vanishing.

We also examined more complicated initial conditions. If one uses three phonons, including one optical phonon, one acoustic phonon with an opposite wavevector, and one additional acoustic phonon, the time averaged current approaches an intermediate value between 0 and its initial value $J(0)$ [for instance, if we add one more transverse acoustic phonon with the same wavevector $-k$, we obtain $J_\infty \approx J(0)/2$] in the limit of small anharmonic coupling. This is a typical behavior for a non-ergodic regime. In the ergodic regime realized for long chains $N \gg 1$ and/or high temperatures $k_B T \gg \hbar\Delta_{opt}$, the fourth order anharmonic interaction [Eq. (15)] leads to the relaxation investigated in Sec. IV B using the semiclassical approach.

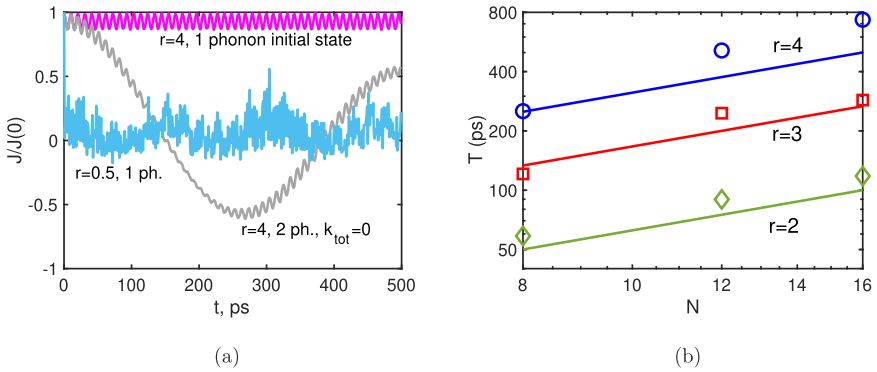

(a) (b)

FIG. 4. Coherent oscillation of current for a two-phonon initial state with the total wavevector 0. (a) Dependence of current on time for one- and two-phonon initial states and bandwidth ratios $r = 1/2$ and 4. The initial state and number of phonons are indicated near each graph. (b) Dependence of oscillation period on chain length at different ratios of bandwidths r for the midband state $n = N/4$ [Eq. (1)]. The straight lines show the expected oscillation period due to resonant interactions in Eq. (27). The anharmonic coupling strength is $V_3 = 0.2\Delta_{opt}$.

B. Semiclassical treatment

1. Semiclassical model

Since most of the experiments are performed at room temperature, the assumption of a low temperature made in Sec. IV A is not satisfied there. At room temperature, a typical thermal energy $k_B T$ is comparable to the acoustic phonon bandwidth and exceeds the optical phonon bandwidth that is usually around 100 cm^{-1}.[21] Under those conditions,

$$\Delta_{opt},\ \Delta_{tr} \le k_B T, \tag{28}$$

we employ a semiclassical treatment of acoustic phonons to simplify the consideration. Here, we use it in the form of Ref. 29 developed to investigate charge transfer in DNA.

The semiclassical approach can be formulated as follows. We describe the optical phonon by the wavefunction within the momentum (wavevector) representation

$$|\psi\rangle = \sum_k c_k |k\rangle, \tag{29}$$

where the symbol $|k\rangle$ stands for the state with the given wavevector k and coefficients c_k are wavefunction amplitudes determining probabilities $P_k = |c_k|^2$ to find the phonon in the state with the given wavevector k, which are subject to the normalization condition $\sum_k P_k = 1$. Transverse phonons are characterized by classical coordinates u_q and momenta p_q also defined in the wavevector representation. We evaluate the current following its definition in Eq. (4) using time-dependent probabilities P_k as $J = \sum_k P_k \partial\omega_{opt}(k)/\partial k$, where the summation is performed over all optical phonon normal modes enumerated by their wavevectors k.

The system is described by the Hamiltonian equation (12),

$$H = \sum_q \frac{p_q p_{-q}}{2M} + \frac{M}{2}\sum_q \omega_{tr}(q)^2 u_q u_{-q} + \sum_k \hbar\omega_{opt}(k) c_k^* c_k + 2V_3\sqrt{2\hbar M\Delta_{tr}}\sum_{k,q} \sin(qa/2)^2 u_q (c_k^* c_{k-q} + C.C.). \tag{30}$$

The time evolution of the variables is defined by Hamilton's equations of motion,

$$\frac{dc_k}{dt} = -\frac{i}{\hbar}\frac{\partial H}{\partial c_k^*},\ \frac{dc_k^*}{dt} = \frac{i}{\hbar}\frac{\partial H}{\partial c_k},\ \frac{du_k}{dt} = \frac{\partial H}{\partial p_{-k}},\ \frac{dp_k}{dt} = -\frac{\partial H}{\partial u_k}. \tag{31}$$

It is straightforward to check that these equations conserve both the total energy and the optical phonon wavefunction normalization $\sum_q |c_k|^2 = 1$. This approximation treats classically all participating phonons. The equations for the amplitudes c_k are equivalent to the Schrödinger equations for the optical phonon interacting with classical transverse acoustic vibrations.

A semiclassical approach is justified for optical phonons if anharmonic interactions are weak compared to harmonic ones,

$$V_3 \ll \Delta_{opt}, \Delta_{tr}. \tag{32}$$

In this regime, one can think of an optical phonon as a plane wave with a certain wavevector k undergoing rare scattering events. This justifies averaging of the nonlinear interactions over the optical phonon wavefunction implied in the classical equations [Eq. (31)]. The semiclassical approach can miss the effect of quantum discreteness,[42] although the analysis of the minimalist system of weakly anharmonically coupled oscillators shows similarity between classical and quantum considerations.[45]

Below, we focus on modeling the relaxation in the regimes of the smallest numbers of sites N, where Fermi's golden rule in the form of Eq. (20) ($N = 20$ and $r < 1$) or Eq. (22) ($N = 48$ and $r > 1$) is still applicable for a reasonable anharmonic coupling strength $V_3 \ge 0.01\Delta_{opt}$. In both cases, we choose the initial midband optical phonon state with the wavevector $k = 2\pi n/L$ and $n = N/4$ with one exception related to the investigation of the dependence of the relaxation rate on the initial state. The dynamics for smaller numbers of sites is slower and contains oscillations determined by rare resonances similarly to Ref. 46. Its consideration is beyond the scope of the present work.

In our calculations, we set the thermal energy equal to the double bandwidth for transverse acoustic phonons $k_B T = 2\hbar\Delta_{tr}$. At that temperature, the classical approximation is reasonably justified, while the temperature under consideration is not much higher than the room temperature where $k_B T \sim \hbar\Delta_{tr}$. The results are applicable to the alkane chains at room temperature only qualitatively, although the theory might be still relevant for other oligomers with narrower bandwidths. One should notice that the semiclassical consideration is developed for the verification of the relevance of the Fermi golden rule estimates of scattering rates. The numerical results below confirm that the optical phonon decoherence emerges in two stages and the decoherence rates can be estimated using the Fermi golden rule.

2. Results of calculations

At time $t = 0$, the optical phonon is placed to the state with a certain wavevector k similarly to Sec. IV A. For transverse acoustic phonons, we choose zero initial coordinates $u_q = 0$ and random momenta $p_q = p_{-q} = \xi_q\sqrt{2Mk_B T}$, where ξ_q are random numbers generated from the Gaussian distribution with a unit width. These initial conditions introduce the relevant temperature if anharmonic interaction is weak [Eq. (31)], so kinetic and potential energies for each normal mode should be approximately equal to $k_B T/2$.

The time dependencies of probabilities $P_k(t) = |c_k(t)|^2$ are calculated solving the Hamiltonian equations [Eq. (31)] and averaging their solutions over many random initial conditions corresponding to the given temperature until the accuracy of few percents is obtained. Below, the results of calculations are reported for time dependent probabilities P_k for different system sizes, anharmonic coupling strengths, and bandwidth ratios r.

First, we report time dependent currents for a representative chain of $N = 20$ sites with an initially excited midband optical phonon. The anharmonic coupling was chosen as $V_3 = 0.05\sqrt{\Delta_{opt}\Delta_{tr}}$ to have bandwidth independent Fermi's golden rule rates of emission and absorption [Eq. (20)]. The absolute value of V_3 and the system size were chosen to avoid discreteness and have perturbation theory applicable. Remember that the temperature is given by $k_B T = 2\hbar\Delta_{tr}$.

Time dependencies of current are very different for $r \le 1$ where it can be characterized by a single relaxation time and $r \ge 2$ where it relaxes in two stages, including the fast initial relaxation during the time of the order of one picosecond and a slow subsequent relaxation taking orders of magnitude longer. This observation is consistent

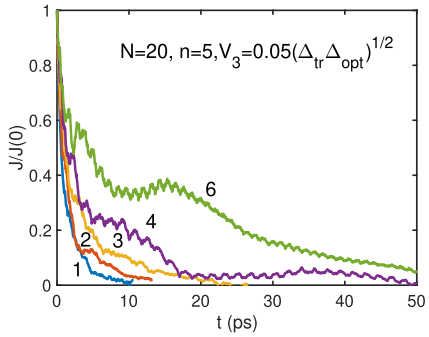

FIG. 5. Time dependence of current for different ratios (r) of acoustic to optical bandwidth indicated near each graph. The temperature is defined as $k_B T = 2\hbar\Delta_{tr}$.

with the expectations of Sec. III A 2. For $N = 20$ and $r > 1$ a system discreteness is significant and it shows up as oscillations in Fig. 5 due to three or four phonon Fermi resonances. We do not consider them in detail.

To characterize both regimes, we examine relaxation time behaviors separately in Sec. IV B 3 for a small bandwidth ratio $r = 1/2$ and in Sec. IV B 4 in the opposite regime of $r > 1$.

3. Relaxation at small bandwidth ratio ($r = 1/2$)

For $r \le 1$, it is natural to expect a population relaxation following the Fermi golden rule predictions at high temperatures [Eq. (20)]. To verify that, we examined the population relaxation for the bandwidth ratio $r = 1/2$ and all possible initial wavevectors k for $N = 20$ as reported in Fig. 6. The relaxation time for each initial state time dependent population $P_n(t)$ corresponding to the wavevector $k = 2\pi n/L$ was estimated setting $P_n(T_{\rm rel}(n)) = P_n(\infty) + (1 - P_n(\infty))e^{-1}$, where $P_n(\infty) \approx 1/N$ is the infinite time limit of the phonon state population in the classical ergodic system. Exact time averaged populations slightly differ from each other for different wavevectors, but this difference is negligible for the temperature under consideration due to the conservation of the number of optical phonons and their classical treatment.

To compare the numerical results for relaxation times with the theory [Eq. (20)] predicting that

$$T_{\rm rel}(n) = \frac{\hbar\Delta_{\rm tr}\Delta_{\rm opt}\,\sin\left(|n|\pi/N\right)}{16V_3^2 k_{\rm B}T},$$

we plot the ratios $T_{\rm rel}(n)/\sin(n\pi/N)$ vs n, which should be independent of the initial wavevector in Fig. 6(a). Only half of initial wavevectors are shown since the data for n and $-n$ are identical due to the inversion symmetry. We did not examine lifetimes of the states with $n = 0$ and $N/2$, where the Fermi golden rule must obviously fail.

According to our observations, the results for the relaxation rate are in an excellent agreement with the theory for $N = 20$ and $2 \le n \le 8$. The deviations at small wavevectors are probably because the predicted relaxation rate is too fast there, so the Fermi golden rule is no longer applicable (see discussion in Sec. III C 1). The dependence of the relaxation time on the anharmonic interaction $T_{\rm rel} \propto V_3^{-2}$ is also consistent with the theory predictions except for very small coupling constants $V_3 \le 0.01\Delta_{\rm opt}$, where discreteness becomes significant as shown in Fig. 6(b).

4. Relaxation at large bandwidth ratio $r > 1$

For a large bandwidth ratio $r \ge 2$, the evolution of current cannot be described using a single relaxation time as it is clearly seen in Fig. 5. The current relaxes in two stages, including the first fast stage taking few picoseconds due to absorption or emission [Eq. (20)] (forward scattering) and the second slow stage that is expected to be determined by much slower phonon scattering [Eq. (22)] (backscattering). Here, we report the results for the slow stage relaxation for $N = 48$ and compare the current evolution at the slow stage with the predictions of theory [Eq. (22)]. We always excite initially the mid-band optical phonon $n = 12$ and use the temperature corresponding to the thermal energy exceeding the transverse phonon bandwidth twice $k_B T = 2\hbar\Delta_{\rm tr}$.

First, we report the results for the representative bandwidth ratio $r = 3$ in Fig. 7. In Fig. 7(a), the time evolution of currents is shown for different anharmonic coupling constants. The current clearly relaxes in two stages, and we focus on the second stage.

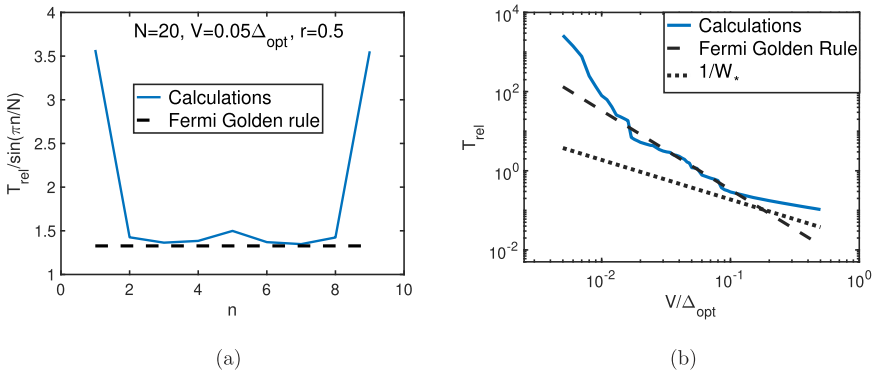

(a) (b)

FIG. 6. (a) Dependence of the rescaled relaxation time on the wavevector for $N = 20$ compared to the Fermi golden rule result [Eq. (20)] for the parameters $k_B T = 2\Delta_{\rm tr}$, $V = 0.05\Delta_{\rm opt}$, and $r = 0.5$. (b) Dependence of the relaxation time on the strength of the anharmonic interaction for the same parameters as in (a) and $n = 5$. Results are compared with the Fermi golden rule [Eq. (20)] (dashed line) and the minimum relaxation time $1/W_*$ [Eq. (25)] (dotted line).

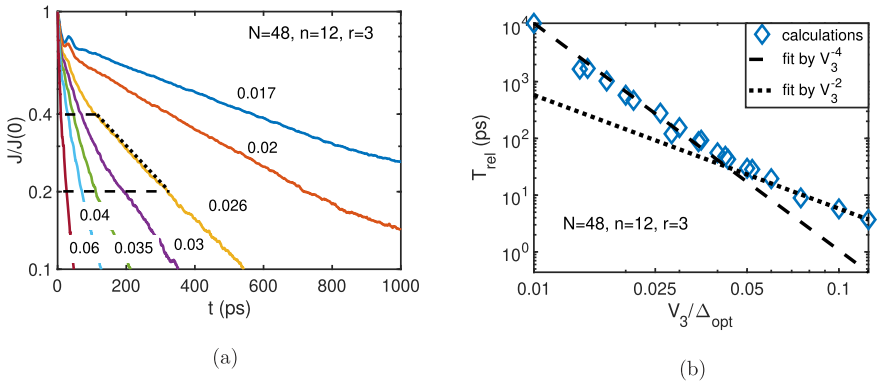

FIG. 7. (a) Time dependence of current for the initially excited midband optical phonon and different anharmonic coupling strengths V_3/Δ_{opt} shown near each curve. The negative inverse slope of the dashed line serves as an estimate for the relaxation time. (b) Dependence of relaxation times on anharmonic coupling strengths fitted by V_3^{-4} dependence for small couplings (dashed line) and V_3^{-2} dependence for large couplings (dotted line). In both graphs, the bandwidth ratio is $r = 3$.

To extract the relaxation time, we fit the current time dependence by a single exponent for the part of relaxation occurring between $J/J(0) = 0.4$ and $J/J(0) = 0.2$ as shown by the dashed line. The relaxation time is estimated using the negative inverse slope of this line. The results are sensitive to the fitting domain [use of the specific points $J/J(0) = 0.4$ and 0.2 to extract the relaxation rate], since relaxation is getting slower with time possibly reflecting its diffusive nature. Our estimate gives a right guess about the time of the transition between ballistic and diffusive regimes and parametric dependencies of this time nearly insensitive to its specific definition.

The relaxation time dependence on the anharmonic coupling strength is shown in Fig. 7. At relatively small coupling $V_3 \le 0.05\Delta_{opt}$, this dependence is perfectly consistent with the theory prediction of the inverse fourth power dependence [Eq. (22)], while at large V, it switches to the weaker dependence probably because of the failure of the Fermi golden rule as a perturbation theory.

Similar scaling of relaxation times is obtained for other two considered bandwidth ratios $r = 2$ and $r = 4$ as illustrated in Figs. 8(a) and 8(b), respectively. The dependence V_3^{-4} is seen in a wider domain for $r = 4$ and in a very narrow domain for $r = 2$ compared to $r = 3$ that is the consequence of different separations from the threshold at $r = 1$.

We also examine the dependence of relaxation times on the bandwidth ratio. In our regime of interest $k_B T = 2\hbar\Delta_{tr}$, the expected dependence can be expressed following Eq. (22) as $T_{rel} = r^5\Delta_{opt}^3/(4CV_3^4)$. To check the relevance of this dependence, we plot the rescaled relaxation times T_{rel}/r^5 in Fig. 9 for $r = 2$, 3, and 4. The graphs for the bandwidth ratios $r = 3$ and 4 are perfectly consistent with the theory expectations. The dependence for $r = 2$ deviates from those expectations. This deviation is possibly because the case $r = 2$ is close to the crossover regime $r = 1$. Two approaches are getting consistent for $r = 2$ at small V_3 if we use the resonant coupling r dependence $V(k, -k, -k, k) \propto 1/(r^2 - 1)$ [see Eq. (27)] to estimate the effective scattering matrix element replacing expected r^5 relaxation time dependence with $r(r^2 - 1)^2$.

Using the numerical estimate of the relaxation time, we can find the dimensionless constant C in Eq. (22) as $2.7 \cdot 10^4$. This dimensionless numerical factor is huge, but this is not so surprising. The typical transition matrix element $V(k, -k, -k, k)$ [Eq. (27)]

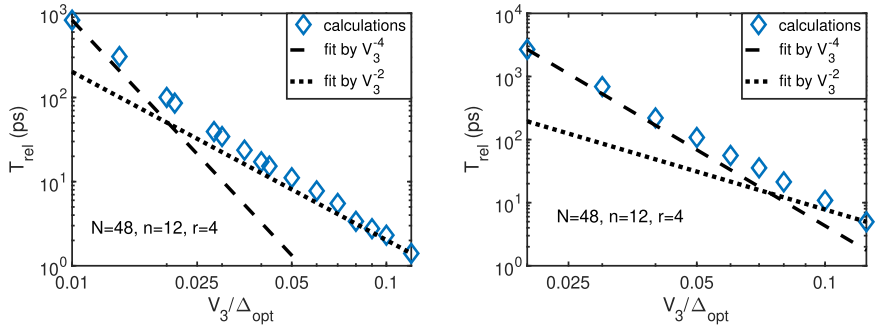

FIG. 8. Dependence of relaxation times on anharmonic coupling strengths for $r = 2$ (a) and $r = 4$ (b) fitted similarly to Fig. 7.

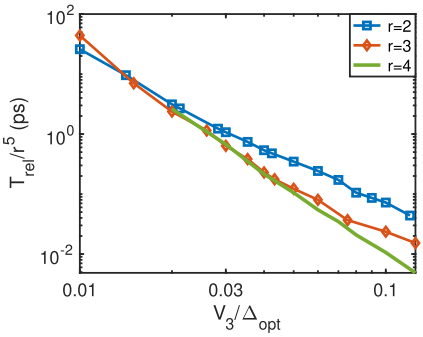

FIG. 9. Dependence of rescaled relaxation times on anharmonic coupling for different bandwidth ratios.

contains a large numerical factor of $\eta_4 = 16$. At high temperature, it also acquires a factor expressing the number of thermal phonons $k_B T/(\hbar\omega_{tr}(k))$ estimated in Eq. (22) as $k_B T/(\hbar\Delta_{tr})$. However, the actual energy $\hbar\omega_{tr}(k)$ for the initial midband state $k = \pi/(2a)$ is a half of the bandwidth, so an extra factor of two naturally appears in the definition of the matrix element modifying the numerical factor to $2\eta_4 \sim 32$. The squared matrix element within the Fermi golden rule acquires this numerical factor squared that is $32^2 \approx 1000$.

The remaining factor of $C/32^2 \approx 27$ in the definition of the current relaxation rate originated from the integration over two wavevectors in the related Fermi-golden rule expression for the current relaxation rate (see Refs. 47 and 48). Another possible origin for the extra rate enhancement factor of order of 10 can be due to a multistep current evolution involving first fast relaxation of the phonon to one of the states with a smaller energy with a subsequent backscattering from that state that can happen faster compared to that from the initial state due to a larger number of participating transverse phonons at lower energies. Thus, the large numerical factor C is quite reasonable for the current relaxation rate.

V. ACCELERATION OF TRANSPORT FOR A SMALL INITIAL VELOCITY OF OPTICAL PHONON

We demonstrated in Secs. III and IV that the evolution of an optical phonon due to its interaction with transverse phonons for the bandwidth ratio (transverse to optical ones) greater than unity can be separated into two stages. In the first, fast stage, the phonon is scattered only forward, so its average velocity remains finite as for the ballistic transport. Consequently, in the first stage, we observed numerically the fast current reduction to some finite value [Fig. 5]. This reduction is because the initial midband state used in Sec. IV possesses the maximum velocity. If the initial state is chosen near band edges, where the velocity approaches minimum, then the forward scattering to other faster states should increase the velocity. This is an interesting and untypical regime, where the relaxation enhances the current.

Such acceleration can possibly explain the recently discovered increase in the optical phonon ballistic transport velocity in alkane chains with the chain length.[27] The measurements carried out similarly to earlier work[21] show that the phonon velocity increases with increasing the chain length from 14 Å/ps for shorter chains to around 48 Å/ps for longer chains containing more than 20 CH_2 groups. If the propagating wavepacket is initiated at the top of a band where the group velocity is small, it can be scattered toward the midband states, featuring much larger group velocities, still propagating in the forward direction. Since such a process became efficient at longer chains where the phonon has sufficient time for scattering, it would result in a speed increase. Several optical bands of alkane chains can fit such conditions, including CH_2 wagging, CH_2 rocking, and C–C stretching bands.[49] Then, in long chains, the phonon gets re-scattered forward to midband states possessing much bigger group velocities up to 60 Å/ps. This redistribution emerges during the first stage of relaxation taking few picoseconds, while the second stage taking time orders of magnitude longer is possibly not reached yet.

To demonstrate the optical phonon acceleration numerically, we tried a variety of model parameters always choosing the initially excited optical phonon with a smallest (yet nonzero) velocity for different numbers of sites N and anharmonic coupling strengths V_3. The high temperature semiclassical regime ($k_B T = 2\hbar\Delta_{tr}$) is considered since we observed a substantial increase in current only for $N > 20$ sites, where an accurate quantum mechanical treatment is problematic. Below, we report a substantial increase in current for $N = 21$ with the initial state wavevector $k = 2\pi n/L$ and $n = 10$ possessing the minimum group velocity.

For our study, we choose an anharmonic coupling strength $V_3 = 0.01\sqrt{\Delta_{opt}\Delta_{tr}}$ for bandwidth ratios 1.5, 2, and 3 similarly to Sec. III B 1. The absolute value of V_3 was chosen using guess and check method to maximize the current rise. The time dependence of current for these specific parameters is shown in Fig. 10(a). The anharmonic interaction V_3 used in calculations is consistent with our DFT estimate[50] of anharmonic interactions of the optical phonons belonging to the most wide rocking band[24] and transverse acoustic phonons in heptane and in the C5 molecule composed of the alkane chain of five CH_2 groups with carboxyl and azido end groups, which was investigated experimentally.[27] In both cases, the typical interaction is of order of few inverse centimeters that is around hundred times smaller than the typical bandwidth. In heptane, around half of anharmonic interactions vanish possibly due to the inversion symmetry, broken in C5 due to the end groups.

According to Fig. 10(a), the current rises in the fast stage taking around 10 ps by a factor of 2 or even 2.5 depending on the specific bandwidth ratio. The slow stage takes orders of magnitude longer, yet it limits the maximum current raise. The strongest increase in current is observed for a smallest considered bandwidth ratio of $r = 1.5$.

The verification of the proposed interpretation of the experimental data can be made modifying the temperature, which is the only controlling parameter that can be changed relatively easily and can be modeled using the present theory. The effect of temperature is reported in Fig. 10(b). The rise of the current and, correspondingly, maximum transport velocity is clearly seen with the reduction in temperature, and it can be probed experimentally to validate the present theory. This rise with decreasing the temperature could be due to the suppression of slow backscattering processes limiting the raise of the current. One should notice, however, that a further reduction in temperature can reduce the transport rate due to

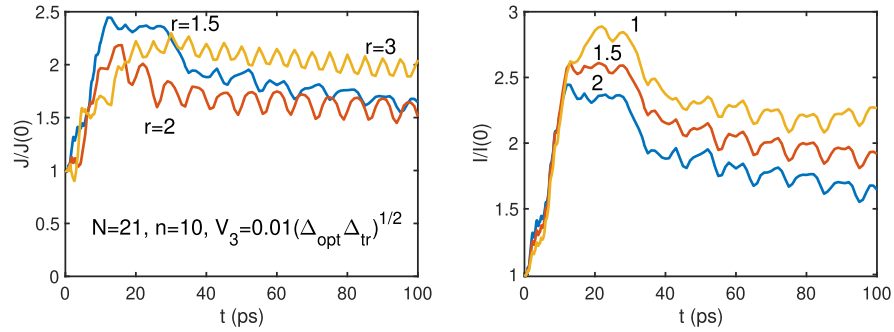

(a) (b)

FIG. 10. (a) Raise of current due to anharmonic interaction for the initial state with a small group velocity ($N = 21$, $n = 10$) and different bandwidth ratios r shown for each graph. The temperature is fixed at $k_B T = 2\hbar\Delta_{tr}$. (b) Current for the bandwidth ratio $r = 1.5$ at different temperatures. The ratio $k_B T/(\hbar\Delta_{tr})$ is shown above each graph.

phonon redistribution toward lower energies corresponding to their Boltzmann distribution.

VI. CONCLUSIONS

We examined the transport and decoherence of optical phonons in periodic chains due to their interaction with transverse acoustic phonons using three different levels of theory. Similarly to earlier work,[17] where the interaction with longitudinal acoustic phonons was considered, we found two distinguishable dynamic regimes depending on the relationship between acoustic and optical phonon bandwidths.

In the typical regime of a narrower optical phonon band compared to acoustic phonon bands, an optical phonon relaxation within the band emerges in two stages. The first stage takes several picoseconds. It includes fast equilibration of the initially excited optical phonon within the band states featuring similarly directed group velocities by means of forward scattering accompanied by absorption or emission of transverse acoustic phonons forbidden for longitudinal phonons due to Cherenkov's constraint.[17] Importantly, this forward only scattering supports the ballistic transport.

If the initial optical phonon group velocity is smaller than the typical optical phonon velocity determined by its average absolute value over all normal modes within the given band, then the phonon accelerates due to forward scattering to the states with a higher velocity. The latter regime is possibly realized in the recent measurements of energy transport through alkane chains, where the optical phonon velocity increases with increasing the chain length.[27] The anharmonic interaction needed to realize this regime is approximately consistent with its numerical estimate for alkane chains. The theory can be verified reducing the temperature that should lead to a stronger increase in the optical phonon velocity.

The second stage of phonon relaxation involves its backscattering. It converts the ballistic transport regime to diffusive but takes a much longer time. The backscattering occurs much slower compared to the forward scattering in the first stage, because for narrow optical bands, it requires higher order anharmonic interactions.

If the acoustic band is narrower (bandwidth ratio r less than unity), then the optical phonon relaxes very quickly in about a few picoseconds from its initial state to all other states within the band. This relaxation leads to the substantial current reduction and changing the transport from ballistic to diffusive.

Usually, acoustic phonon bands are wider compared to optical phonon bands.[17,21] However, our results for the opposite regime are also relevant for other systems of interest, including electrons propagating in periodic molecules. The electron energy band can be broader than any phonon band, so the situation of $r < 1$ is quite realistic.

ACKNOWLEDGMENTS

This work was supported by the National Science Foundation (Grant No. CHE-2201027).

AUTHOR DECLARATIONS

Conflict of Interest

The authors have no conflicts to disclose.

Author Contributions

Alexander L. Burin: Conceptualization (equal); Formal analysis (equal); Funding acquisition (equal); Investigation (equal); Methodology (equal); Project administration (equal); Software (equal); Writing – original draft (equal). **Igor V. Rubtsov**: Conceptualization (equal); Data curation (equal); Investigation (equal); Project administration (equal); Validation (equal); Writing – review & editing (equal).

DATA AVAILABILITY

The data that support the findings of this study are available from the corresponding author upon reasonable request.

REFERENCES

[1] A. Nitzan, "Molecules take the heat," Science **317**, 759–760 (2007).
[2] D. M. Leitner, "Quantum ergodicity and energy flow in molecules," Adv. Phys. **64**, 445–517 (2015).

[3]H. D. Pandey and D. M. Leitner, "Thermalization and thermal transport in molecules," J. Phys. Chem. Lett. **7**, 5062–5067 (2016).
[4]D. M. Leitner, H. D. Pandey, and K. M. Reid, "Energy transport across interfaces in biomolecular systems," J. Phys. Chem. B **123**, 9507–9524 (2019).
[5]S. Karmakar and S. Keshavamurthy, "Intramolecular vibrational energy redistribution and the quantum ergodicity transition: A phase space perspective," Phys. Chem. Chem. Phys. **22**, 11139–11173 (2020).
[6]J. P. T. Zaragoza, A. R. Offenbacher, S. Hu, C. L. Gee, Z. M. Firestein, N. Minnetian, Z. Deng, F. Fan, A. T. Iavarone, and J. P. Klinman, "Temporal and spatial resolution of distal protein motions that activate hydrogen tunneling in soybean lipoxygenase," Proc. Natl. Acad. Sci. U. S. A. **120**, e2211630120 (2023).
[7]Y. Jiang, L. C. Liu, A. Sarracini, K. M. Krawczyk, J. S. Wentzell, C. Lu, R. L. Field, S. F. Matar, W. Gawelda, H. M. Müller-Werkmeister, and R. J. D. Miller, "Direct observation of nuclear reorganization driven by ultrafast spin transitions," Nat. Commun. **11**, 1530 (2020).
[8]T. Zhu, K. Swaminathan-Gopalan, K. J. Cruse, K. Stephani, and E. Ertekin, "Vibrational energy transport in hybrid ordered/disordered nanocomposites: Hybridization and avoided crossings of localized and delocalized modes," Adv. Funct. Mater. **28**, 1706268 (2018).
[9]D. Segal, A. Nitzan, and P. Hänggi, "Thermal conductance through molecular wires," J. Chem. Phys. **119**, 6840–6855 (2003).
[10]Z. Wang, J. A. Carter, A. Lagutchev, Y. K. Koh, N.-H. Seong, D. G. Cahill, and D. D. Dlott, "Ultrafast flash thermal conductance of molecular chains," Science **317**, 787–790 (2007).
[11]A. Henry and G. Chen, "High thermal conductivity of single polyethylene chains using molecular dynamics simulations," Phys. Rev. Lett. **101**, 235502 (2008).
[12]D. Segal and B. K. Agarwalla, "Vibrational heat transport in molecular junctions," Annu. Rev. Phys. Chem. **67**, 185–209 (2016).
[13]R. Chen, I. Sharony, and A. Nitzan, "Local atomic heat currents and classical interference in single-molecule heat conduction," J. Phys. Chem. Lett. **11**, 4261–4268 (2020).
[14]B. Gotsmann, A. Gemma, and D. Segal, "Quantum phonon transport through channels and molecules—A Perspective," Appl. Phys. Lett. **120**, 160503 (2022).
[15]I. V. Rubtsov and A. L. Burin, "Ballistic and diffusive vibrational energy transport in molecules," J. Chem. Phys. **150**, 020901 (2019).
[16]L. Cui, S. Hur, Z. A. Akbar *et al.*, "Thermal conductance of single-molecule junctions," Nature **572**, 628–633 (2019).
[17]A. L. Burin, I. V. Parshin, and I. V. Rubtsov, "Maximum propagation speed and Cherenkov effect in optical phonon transport through periodic molecular chains," J. Chem. Phys. **159**, 054903 (2023).
[18]I. V. Rubtsov, "Relaxation-assisted two-dimensional infrared (RA 2DIR) method: Accessing distances over 10 Å and measuring bond connectivity patterns," Acc. Chem. Res. **42**, 1385–1394 (2009).
[19]N. I. Rubtsova, L. N. Qasim, A. A. Kurnosov, A. L. Burin, and I. V. Rubtsov, "Ballistic energy transport in oligomers," Acc. Chem. Res. **48**, 2547–2555 (2015).
[20]T. X. Leong, L. N. Qasim, R. T. Mackin, Y. Du, R. A. Pascal, and I. V. Rubtsov, "Unidirectional coherent energy transport via conjugated oligo(*p*-phenylene) chains," J. Chem. Phys. **154**, 134304 (2021).
[21]N. I. Rubtsova, C. M. Nyby, H. Zhang, B. Zhang, X. Zhou, J. Jayawickramarajah, A. L. Burin, and I. V. Rubtsov, "Room-temperature ballistic energy transport in molecules with repeating units," J. Chem. Phys. **142**, 212412 (2015).
[22]L. N. Qasim, E. B. Atuk, A. O. Maksymov, J. Jayawickramarajah, A. L. Burin, and I. V. Rubtsov, "Ballistic transport of vibrational energy through an amide group bridging alkyl chains," J. Phys. Chem. C **123**, 3381–3392 (2019).
[23]A. A. Kurnosov, I. V. Rubtsov, and A. L. Burin, "Communication: Fast transport and relaxation of vibrational energy in polymer chains," J. Chem. Phys. **142**, 011101 (2015).
[24]N. I. Rubtsova, A. A. Kurnosov, A. L. Burin, and I. V. Rubtsov, "Temperature dependence of the ballistic energy transport in perfluoroalkanes," J. Phys. Chem. B **118**, 8381–8387 (2014).
[25]L. N. Qasim, A. Kurnosov, Y. Yue, Z. Lin, A. L. Burin, and I. V. Rubtsov, "Energy transport in peg oligomers: Contributions of different optical bands," J. Phys. Chem. C **120**, 26663–26677 (2016).
[26]A. Boulatov and A. L. Burin, "Crucial effect of transverse vibrations on the transport through polymer chains," J. Chem. Phys. **153**, 134102 (2020).
[27]S. U. Nawagamuwage, E. S. Williams, M. M. Islam, I. V. Parshin, A. L. Burin, N. Busschaert, and I. V. Rubtsov, "Ballistic energy transport via long alkyl chains: A new initiation mechanism," J. Phys. Chem. B (to be published) (2024); arXiv:2405.13776 [physics.chem-ph].
[28]A. Burin, A. O. Maksymov, M. Schmidt, and I. Y. Polishchuk, "Chaotic dynamics in a quantum Fermi-Pasta-Ulam problem," Entropy **21**, 51 (2019).
[29]K. Senthilkumar, F. C. Grozema, C. F. Guerra, F. M. Bickelhaupt, F. D. Lewis, Y. A. Berlin, M. A. Ratner, and L. D. A. Siebbeles, "Absolute rates of hole transfer in DNA," J. Am. Chem. Soc. **127**, 14894–14903 (2005).
[30]X. Duan, Z. Li, J. Liu, G. Chen, and X. Li, "Roles of kink on the thermal transport in single polyethylene chains," J. Appl. Phys. **125**, 164303 (2019).
[31]Y. Yue, L. N. Qasim, A. A. Kurnosov, N. I. Rubtsova, R. T. Mackin, H. Zhang, B. Zhang, X. Zhou, J. Jayawickramarajah, A. L. Burin, and I. V. Rubtsov, "Band-selective ballistic energy transport in alkane oligomers: Toward controlling the transport speed," J. Phys. Chem. B **119**, 6448–6456 (2015).
[32]L. D. Landau, E. M. Lifšic, E. M. Lifshitz, A. M. Kosevich, J. B. Sykes, L. P. Pitaevskii, and W. H. Reid, *Theory of Elasticity*, *Vol. 7 Course of Theoretical Physics* (Elsevier Science, 1986).
[33]G. Hartwig, *Polymer Properties at Room and Cryogenic Temperatures* (Springer, Boston, MA, 1994), pp. 17–46.
[34]L. Chico, R. Pérez-Álvarez, and C. Cabrillo, "Low-frequency phonons in carbon nanotubes: A continuum approach," Phys. Rev. B **73**, 075425 (2006).
[35]R. F. Gibson, E. O. Ayorinde, and Y.-F. Wen, "Vibrations of carbon nanotubes and their composites: A review," Compos. Sci. Technol. **67**, 1–28 (2007).
[36]C. Kittel, *Introduction to Solid State Physics*, 8th ed. (Wiley, 2004).
[37]R. Borrelli and M. F. Gelin, "Quantum dynamics of vibrational energy flow in oscillator chains driven by anharmonic interactions," New J. Phys. **22**, 123002 (2020).
[38]J. H. Van Vleck, "On ??-Type doubling and electron spin in the spectra of diatomic molecules," Phys. Rev. **33**, 467 (1929).
[39]S. G. Ramesh, E. L. Sibert III, and L. Edwin, "Combined perturbative-variational investigation of the vibrations of $CHBr_3$ and $CDBr_3$," J. Chem. Phys. **120**, 11011–11025 (2004).
[40]J. R. Schrieffer and P. A. Wolff, "Relation between the Anderson and Kondo Hamiltonians," Phys. Rev. **149**, 491–492 (1966).
[41]D. M. Leitner, "Vibrational energy transfer in helices," Phys. Rev. Lett. **87**, 188102 (2001).
[42]D. M. Leitner and P. G. Wolynes, "Quantization of the stochastic pump model of Arnold diffusion," Phys. Rev. Lett. **79**, 55–58 (1997).
[43]D. E. Logan and P. G. Wolynes, "Quantum localization and energy flow in many-dimensional Fermi resonant systems," J. Chem. Phys. **93**, 4994–5012 (1990).
[44]V. L. Berezinskii and L. P. Gor'kov, "On the theory of electrons localized in the field of defects," Zh. Eksp. Teor. Fiz. **77**, 2498 (1979) [J. Exp. Theor. Phys. **50**, 1209 (1979)].
[45]I. Tikhonenkov, A. Vardi, J. R. Anglin, and D. Cohen, "Minimal Fokker-Planck theory for the thermalization of mesoscopic subsystems," Phys. Rev. Lett. **110**, 050401 (2013).
[46]M. Onorato, L. Vozella, D. Proment, and Y. V. Lvov, "Route to thermalization in the α -Fermi–Pasta–Ulam system," Proc. Natl. Acad. Sci. U. S. A. **112**, 4208–4213 (2015).
[47]L. P. Pitaevskii and E. M. Lifshitz, *Physical Kinetics* (Elsevier Science, 2012), Vol. 10.
[48]K. Busch, C. M. Soukoulis, and E. N. Economou, "Transport and scattering mean free paths of classical waves," Phys. Rev. B **50**, 93–98 (1994).
[49]S. U. Nawagamuwage, L. N. Qasim, X. Zhou, T. X. Leong, I. V. Parshin, J. Jayawickramarajah, A. L. Burin, and I. V. Rubtsov, "Competition of several energy-transport initiation mechanisms defines the ballistic transport speed," J. Phys. Chem. B **125**, 7546–7555 (2021).
[50]S. L. Tesar, V. M. Kasyanenko, I. V. Rubtsov, G. I. Rubtsov, and A. L. Burin, "Theoretical study of internal vibrational relaxation and energy transport in polyatomic molecules," J. Phys. Chem. A **117**, 315–323 (2013).